frontiers in Materials

ORIGINAL RESEARCH
published: 14 August 2020
doi: 10.3389/fmats.2020.00269

Cellulose-Based Solid Electrolyte Membranes Through Microwave Assisted Regeneration and Application in Electrochromic Displays

*Paulo Duarte[1], Sónia Pereira[1], Inês Cunha[1], Ana Pimentel[1], Madalena Dionísio[2], Elvira Fortunato[1], Rodrigo Martins[1] and Luís Pereira[1]**

[1] CENIMAT/I3N and CEMOP-UNINOVA, Departamento de Ciência dos Materiais, Faculdade de Ciências e Tecnologia, Universidade Nova de Lisboa, Caparica, Portugal, [2] REQUIMTE, Departamento de Química, Faculdade de Ciências e Tecnologia, Universidade Nova de Lisboa, Caparica, Portugal

OPEN ACCESS

Edited by:
Brahim Aissa, MPB Technologies & Communications, Canada

Reviewed by:
Jianbo Yin, Northwestern Polytechnical University, China
Tongqing Lu, Xi'an Jiaotong University, China

***Correspondence:**
Luís Pereira
lmnp@fct.unl.pt

Specialty section:
This article was submitted to Smart Materials, a section of the journal Frontiers in Materials

Received: *25 October 2019*
Accepted: *20 July 2020*
Published: *14 August 2020*

Citation:
Duarte P, Pereira S, Cunha I, Pimentel A, Dionísio M, Fortunato E, Martins R and Pereira L (2020) Cellulose-Based Solid Electrolyte Membranes Through Microwave Assisted Regeneration and Application in Electrochromic Displays. Front. Mater. 7:269. doi: 10.3389/fmats.2020.00269

One of the most current trends in applied electrochemistry is the development of solid ionic conductors with electrical, mechanical, and optical properties tailored for a specific functional application. Moreover, particular interest exists in materials with low environmental impact and low cost where matters such as sustainability and recyclability are considered. In this study, these concerns were considered by developing a solid-state electrolyte based on regenerated cellulose that meets the requirements for application in electrochromic devices. This soft-matter electrolyte exhibits particularly high room temperature ionic conductivity in the range of 6.5 mS cm^{-1} and Young's modulus in the range 3.7 GPa. Optimized electrolyte membranes were applied to inorganic optically active films resulting in all-solid-state electrochromic devices with performances reaching a practical level, retaining its optical modulation characteristics after hundreds of cycles.

Keywords: cellulose, solid electrolytes, microwave synthesis, regeneration, electrochromic displays

INTRODUCTION

Quasi-solid soft matter and polymer solid-state electrolytes have been subject of extensive research aiming to replace liquid electrolytes in some relevant applications such as ion rechargeable batteries (Amici et al., 2019; Choudhury et al., 2019), fuel cells (Ahn et al., 2020), electrochromic displays/windows (Vidinha et al., 2008; Garino et al., 2013; Fernandes et al., 2014), and electrolyte-gated transistors (Cunha et al., 2017; Nketia-Yawson et al., 2019). The great challenge is on getting high ionic conductivity without the need for a liquid medium or soft membrane separating electrodes. Only then, the problems related to liquid electrolytes, such as leakage, flammability, and toxicity, can be effectively avoided when used in electrochemical devices (Alarco et al., 2004; Lalia et al., 2014).

Two of the most widely employed approaches for solid-state electrolyte formulation have been (i) polymer doping with organic or inorganic salt resulting in so-called polymer electrolytes such as those based on poly(ethylene oxide) (PEO) (Xue et al., 2015; Chen et al., 2019), poly(propylene

oxide) (Han et al., 2017), or poly(ethylene)glycol (PEG) (Asghar et al., 2012; Ji et al., 2017); and (ii) the use of polymer network as mechanical support for ion-conducting matrix, called a composite electrolyte. The last are of particular interest when aiming the improvement of the electrical properties through the addition of inorganic fillers (Ramos et al., 2013; Ji et al., 2017; Zhang et al., 2018) and plastic crystals (Fan et al., 2007; Zhang et al., 2017), and/or the mechanical properties that are achieved by the addition of cross-linked UV-curable polyethylene glycol (di)methacrylate [PEG(D)MA] (Gerbaldi et al., 2009; Choudhury et al., 2019) or ethoxylated trimethylolpropane triacrylate (Fan et al., 2018; Liu et al., 2019).

Within this context, the increasing demand for low cost and more environmentally friendly and sustainable electrolytes leads to the integration of natural polymer hosts with excellent chemical stability and mechanical properties, such as cellulose and its derivatives (Irimia-Vladu, 2014). Some authors have investigated the effect of cellulose in some composite materials based on ionic liquids (Li et al., 2011), methacrylic polymer (Chiappone et al., 2013), PEG (Zhao et al., 2020), or PEO fibers (Samad et al., 2013). Although these composites present excellent ionic conductivities, they need complex synthesis processes. At the same time, the final content of cellulose is also low, being used typically as mechanical strengthen of gel-like electrolytes and improve thermal stability (Zhang et al., 2013; Du et al., 2019). However, cellulose can dissociate lithium salts, adsorb and retain the organic solvents, and accelerate the migration of lithium ions (Zhang et al., 2013; Du et al., 2019; Zhu et al., 2019).

Having in mind what was said above, the work herein presented describes a new and fast synthesis route to obtain a fully cellulose matrix solid electrolyte, with high ionic conductivity, suitable to be used in electrochemical devices. Microwave irradiation has been widely used in cellulose to assist its acid hydrolysis (Ni et al., 2014; Sun et al., 2015). The application to fully cellulose matrix electrolytes is not so explored. Thus, the process introduced here consists of dissolving microcrystalline cellulose (MCC) in N,N-dimethylacetamide (DMAc) and lithium chloride (LiCl) and then employ microwave irradiation to regenerate it before the solvent evaporation step.

MATERIALS AND METHODS

Electrolyte Preparation

MCC (powder 20 μm; Sigma–Aldrich), DMAc (≥99.5% GC from Sigma–Aldrich), and LiCl (98% Panreac) were used as received. The cellulose was dissolved by preparing a solution with a mass ratio of DMAc:MCC:LiCl to 1:0.33:0.1. The solution was then subjected to microwave radiation in a CEM Discovery SP, at 65°C with a maximum power of 50 W, for less than 25 min. The films of the cellulose solid electrolyte (CSE) were obtained by solvent evaporation method at room temperature. For comparison purposes, samples without microwave radiation were prepared following the same procedure. After the solvent evaporation, a very fragile membrane was obtained (CSE/without). This membrane was subjected to a washing step with water (CSE/washed) and dried again at room temperature.

Electrolyte Characterization

The structural analysis of the CSE was made by X-ray diffraction (XRD) using a PANalytical X'Pert PRO diffractometer, equipped with an X'Celerator detector, in a Bragg–Brentano geometry with Cu Kα line radiation (λ = 1.5406 Å). The 2θ scans were performed from 10° to 40°, with a step size of 0.02°. The attenuated total reflectance Fourier transform infrared (FTIR) spectra of the samples were recorded by a Thermo-Nicolet 6700 spectrometer from Thermo Electron Corporation at room temperature. The measurements were carried out in the wavenumber range from 400 to 4,500 cm^{-1} accumulating 64 scans having a resolution of 4 cm^{-1}. Thermogravimetric (TG) measurements were carried out with a Simultaneous Thermal Analyzer (TGA-DSC – STA 449 F3 Jupiter from Netzsch), under air atmosphere and loading 5 mg of each sample into a covered aluminum crucible. The samples were heated from room temperature to 500°C, with a heating rate of 5 K min^{-1}. Conductivity spectra were measured by an impedance analyzer Alpha-N from Novocontrol GmbH, covering a frequency range from 10-1 to 1 MHz, and were collected between −100° and 200°C in steps of 50°C. The samples were placed between two gold plated electrodes (diameter 10 mm). The temperature control was ensured by the Quatro Cryosystem, supplied by Novocontrol, and performed within ± 0.5 K. The mechanical properties of CSE were determined using a tensile testing machine from Rheometric Scientific (Minimat Firmware 3.1).

Electrochromic Display Assembly

As illustrated in **Figure 1**, the CSE was integrated in an electrochromic device (ECD). The CSE was sandwiched between two active layers (tungsten and nickel oxides—WO_3 and NiO, respectively) both deposited on commercial indium tin oxide–coated glass (Xian Yan Technology). The WO_3 films were prepared at room temperature by radiofrequency magnetron sputtering (Pfeiffer Balzer 500). The films were obtained from a tungsten oxide target with a purity of 99.95% under a reactive atmosphere with an oxygen partial pressure of 0.1 Pa and an argon partial pressure of 1.9 Pa. The deposition pressure was 2 Pa with a distance between target and substrate of 15 cm, with a applied power of 200 W for 30 min to obtain films with 300 nm. NiO thin films were deposited at room temperature by e-beam evaporation, in a homemade system, using NiO commercial pellets [random pieces 3–6 mm, 99.99% purity from SCM (Super Conductor Materials)]. The initial chamber pressure was 7×10^{-4} Pa and the growth rate was around 6 nm min^{-1}, to achieve 300 nm thickness (Zhu et al., 2019).

Electrochromic Display Testing

The optical reflectance of the ECDs was measured using a UV-VIS-NIR spectrophotometer (Perkin-Elmer lambda 950) between 250 and 900 nm and the *in situ* reflectance changes at 550 nm were measured combining the same apparatus with a potentiostat (Gamry reference 600) performing cyclic voltammetry between −2.5 and 4 V with a scan rate of 5 mV s^{-1} for 100 cycles.

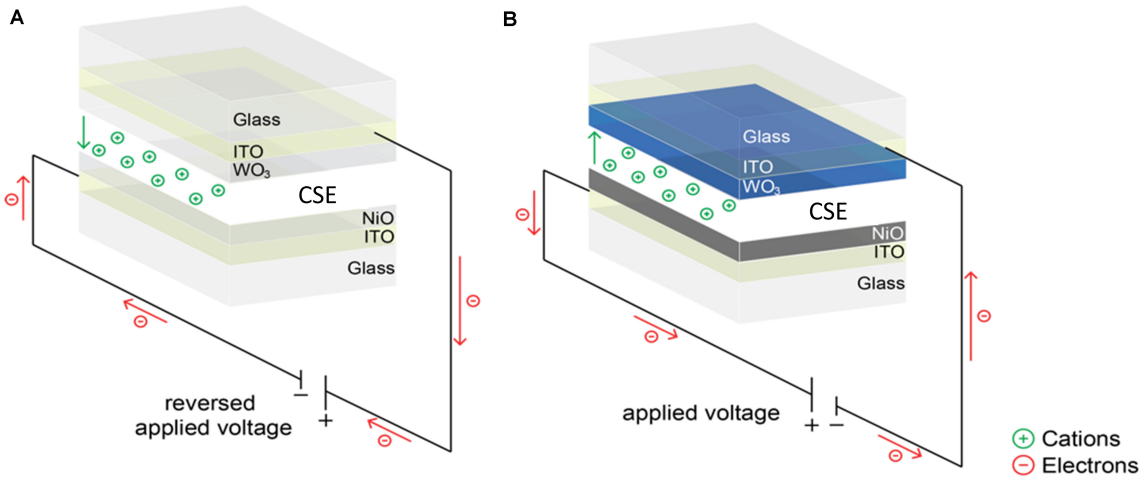

FIGURE 1 | Schematic representation of the electrochromic devices (ECD) produced (Glass/ITO/WO3/CSE/NiO/ITO/Glass) in the: **(A)** bleached and **(B)** colored state.

RESULTS AND DISCUSSION

Electrolyte

Figure 2A compares the XRD patterns of the regenerated CSE and the starting MCC, granules whereas **Figure 2B** shows the diffraction patterns of sample regenerated without microwave radiation (CSE/without) and the same sample after washing with water (CSE/washed). All samples are cellulose type Ia with monoclinic structure (ICDD 00-056-1718) with the characteristic cellulose peaks associated to the planes (-110), (110), and (200) for 2θ values of 14.8°, 16.6°, and 22.9°, respectively. The crystallinity index (CI) was determined by the empirical method proposed by Segal et al. (1959), using the equation:

$$\mathrm{CI}\ (\%) = \frac{\mathrm{I}_{200} - \mathrm{I}_{\mathrm{am}}}{\mathrm{I}_{200}} \times 100 \qquad (1)$$

where I_{200} is the maximum intensity (arbitrary units) of the diffraction peak of the (200) planes, and I_{am} is the minimum intensity taken at a 2θ angle between 18° and 20°, representing the diffraction of the amorphous fraction.

The CI of the CSE/without and CSE is very similar (50 and 53%, respectively), whereas it reaches about 77% for both pristine MCC and CSE/washed samples. This reveals a loss of crystallinity when regenerating the cellulose after dissolving it in the DMAc/LiCl solvent system and not washing them with water, that is, when solvent may remain entrapped inside the formed membrane. However, the most relevant fact is that microwave irradiation (CSE membranes) promotes partial polymerization with similar crystallinity when comparing with normal regeneration (CSE/without membranes), but with much better mechanical properties, because CSE/without results in gel-like samples with no mechanical stiffness. The crystallinity of CSE/without sample can be improved by washing it with water, confirming that the decrease in crystallinity resulting from the presence of DMAc/LiCl entrapped in the regenerated films can be mitigated by microwave assisted regeneration.

FTIR spectra of the original MCC granules and the CSE are presented in **Figure 2C** and samples CSE/without and CSE/washed in **Figure 2D**. The same characteristic FTIR bands were observed for all samples, i.e., O-H, C-H, and C-O stretching mode at 3,400, 2,900, and 1,060 cm^{-1}, respectively. Because the intensity of the 2,900 cm^{-1} band is quite insensitive to variations in the composition, crystallinity, and water content of the cellulose (Łojewska et al., 2005; Pereira L. et al., 2014), it can be used to normalize the spectra (not shown) and evaluate the variation in the intensity of the 3,000–3,600 cm^{-1} band. By doing so, the normalized intensity is the highest in CSE, then in CSE/without, then in CSE/washed, and the lowest for MCC. The increased density of O-H groups suggests the water content in the regenerated membranes follows the same order. A clear difference exists in the FTIR spectra in the band at ∼1,650 cm^{-1}, associated with the asymmetrical C = O stretching of DMAc. It does exist for MCC, as expected, and it is lower in intensity and blue-shifted for CSE when compared with CSE/without and CSE/washed. First, this indicates that there is entrapped solvent even in washed samples. Second, it suggests that the interaction between the entrapped solvent and the cellobiose units is different when microwave irradiation is used. The blue shift in this band for CSE can be associated with lower interaction between DMAc and Li^+ (Zhang et al., 2014; Kotov et al., 2018) and also less interaction between DMAc molecules (Kotov et al., 2018). Both phenomena are coherent with heating promoted by microwave irradiation that reduces solvation of the Li^+ and stoichiometry of the [$(DMAc)_x$-LiCl] complexes, moving from DMAc dimmers toward DMAc monomers. This leaves more DMAc free to become hydrated and increased water uptake capability of the CSE membranes. It worth mentioning that the energetic stability of water H-bonds in the amide hydration sphere is among the higher ones determined for simple amides (Panuszko et al., 2008).

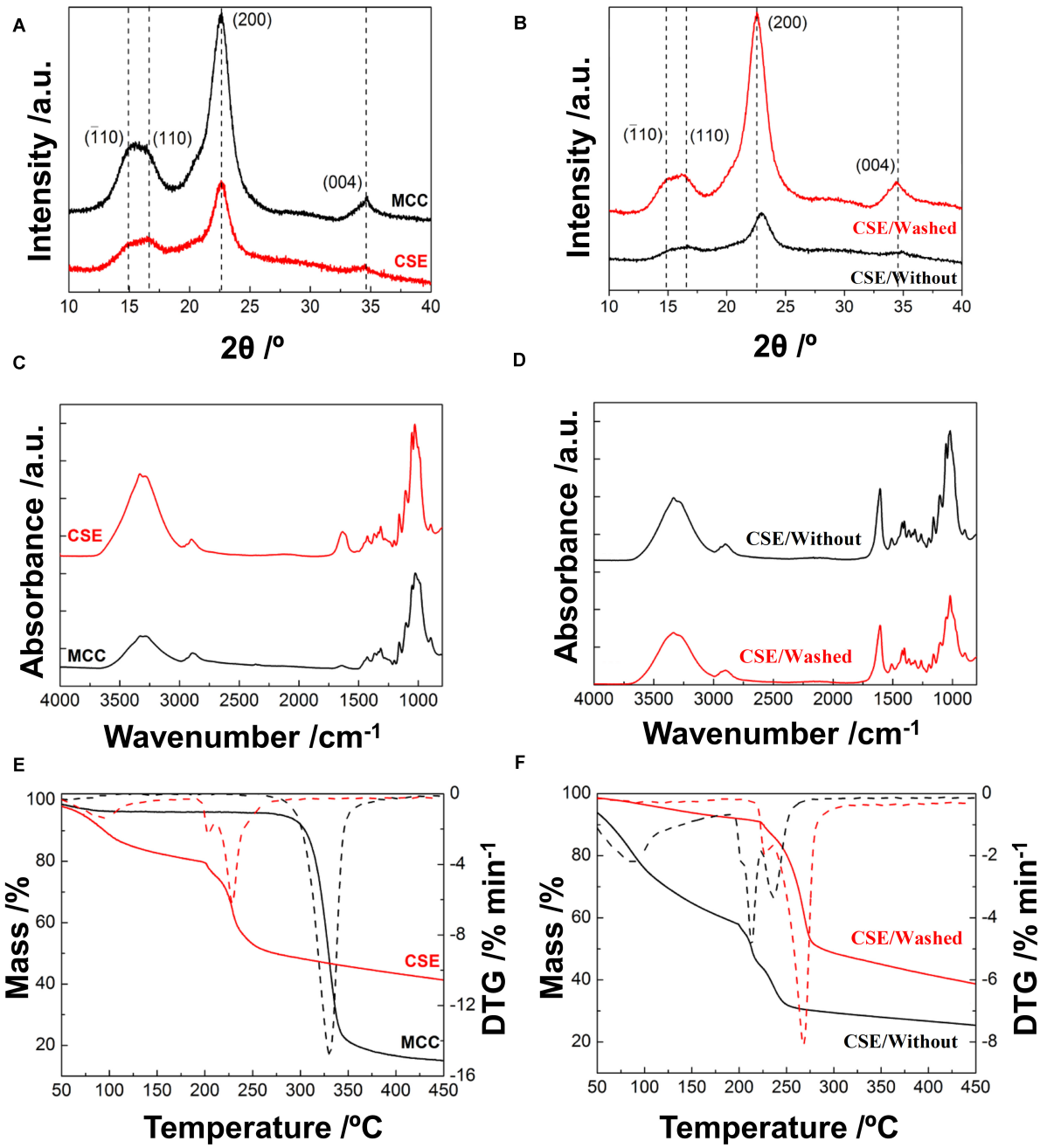

FIGURE 2 | X-ray diffraction patterns of **(A)** source MCC and CSE obtained using microwave irradiation and **(B)** of CSE washed and obtained without microwave irradiation. FTIR spectra of **(C)** source MCC and CSE obtained using microwave irradiation and **(D)** of CSE washed and obtained without microwave irradiation. Thermogravimetric curves (solid lines) and derivative thermogravimetric curves (dash lines) of **(E)** source MCC and CSE obtained using microwave irradiation and **(F)** of CSE washed and obtained without microwave irradiation.

The weight loss curves determined by TGA/DSC are represented in **Figures 2E,F**. For the MCC granules, a small weight loss (3.85%) occurs below 100°C due to the desorption of water while thermal degradation of the cellulose starts around 330°C, where the major weight loss occurs (∼83%). For all the CSE samples, the weight loss below 100°C is much more pronounced supporting the existence of entrapped solvent. This is less pronounced for the CSE/washed membrane due to removal of part of entrapped solvent (not all as shown by FTIR data) during the washing step. When comparing non-washed membranes, the weight loss is lower for CSE when compared with CSE/without, which is consistent with less solvent entrapped and also different hydration of the [$(DMAc)_x$ – LiCl] complexes when microwave radiation is used to assist regeneration. The

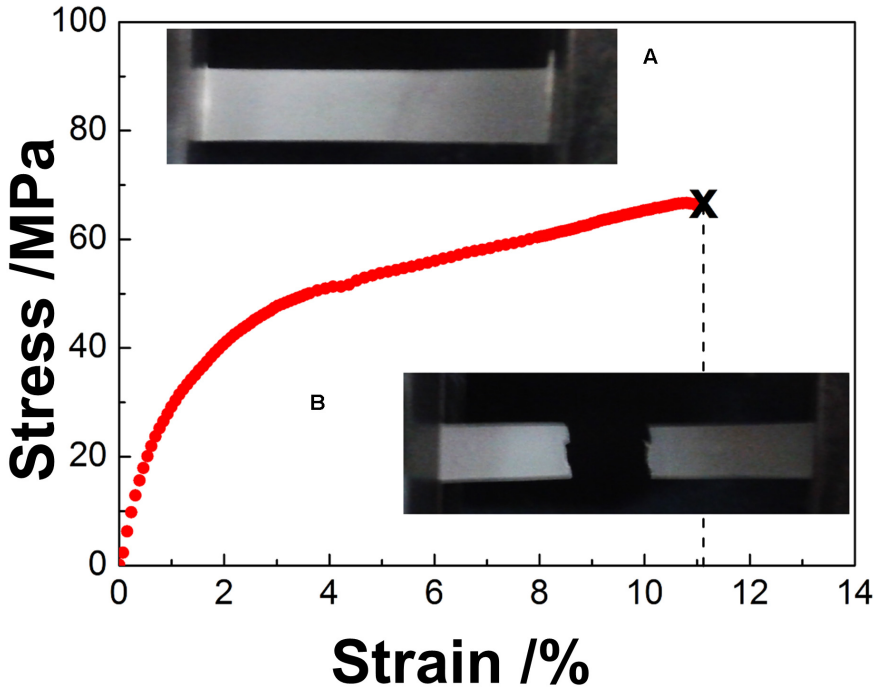

FIGURE 3 | Stress-strain curve of CSE [inset: digital photographs of **(A)** beginning of the test and **(B)** after fracture].

thermal stability of these non-washed membranes is lower when compared with washed ones and MCC granules due to lower crystallinity.

A standard tensile test was carried out on the CSE sample (**Figure 3**). Again, it is worth highlighting that it was not possible to form stiff films from CSE/without and CSE/washed samples. A Young's modulus of 3.7 GPa was obtained, which can be explained by the presence of residual solvent trapped in the cellulosic matrix (confirmed by TGA in **Figure 2E**), as already reported by other authors in some cellulosic regenerated films (Mahadeva et al., 2013). Nevertheless, the yield strength obtained (41.9 MPa) is more than twice that reported in the same work (Mahadeva et al., 2013) and similar to chemically cross-linked cellulose electrolytes (Du et al., 2019), which can be attributed to the partial polymerization promoted by the microwave radiation process. It is possible to speculate that the membranes may become slightly more fragile and have a reduction on the elongation to break after some time. This was not possible to notice by handling them after 1 month. However, this assumption is made based on the small variation of the ionic conductivity (to be discussed below), suggesting some small variation in the water content. This is expected to slightly affect also the mechanical properties of the membranes.

The ionic conductivity measurements of CSE at near room temperature (~20°C) for as regenerated and after 1 month are shown in **Figure 4A**, where the real part of conductivity (σ') is represented as a function of frequency, ω (in log–log scale). The spectra have a *dc* conductivity (σ_{dc}) plateau at higher frequencies (10^4–10^6 Hz) and a conductivity dispersion at lower frequencies (Kremer and Schönhals, 2003; Wang et al., 2013; Yildirim et al., 2018). This behavior at low frequencies can be explained by electrode polarization due to the formation of electric double layers originated by the blocking of charge carriers at the sample/electrode interfaces (Kremer and Schönhals, 2003; Vidinha et al., 2008; Yildirim et al., 2018). The CSE has a σ_{dc} of 6.5 mS.cm^{-1} after synthesis that slightly decreases to 5.2 mS.cm^{-1} after 1 month, which is still an impressive value for a solid-state electrolyte. The CSE maintains the frequency response at room temperature, which confirms its electrochemical stability over such period.

At −90°C, the CSE has the typical behavior of disordered materials such as ionic glasses, ion conducting polymers, and electron-conducting conjugated polymers (Kremer and Schönhals, 2003; Yildirim et al., 2018) with *dc* plateau at low frequencies (shown in **Figure 4B**), but the electrode polarization starts to be visible as the temperature increases. In the temperature range where the spectra have a *dc* plateau in the low and middle-frequency region, it is possible to estimate the σ_{dc} by fitting the Jonscher equation (Jonscher, 1990):

$$\sigma'(\omega) = \sigma_{dc} + A\omega^n \quad (2)$$

where *A* is the pre-exponential factor and n is the fractional exponent ($0.5 \leq n \leq 1$) (Kremer and Schönhals, 2003). The fit of Eq. (2) to the measured real conductivity at −90°C is represented in **Figure 4C** (solid line) and a σ_{dc} of 1.14×10^{-6} mS.cm^{-1} was extracted, which matches well with the value extracted from the plateau. The temperature dependence of the σ_{dc} values is plotted in **Figure 4D**. The empirical Vogel–Fulcher–Tammann (Carvalho et al., 2012; Ledwon et al., 2015) equation was fitted

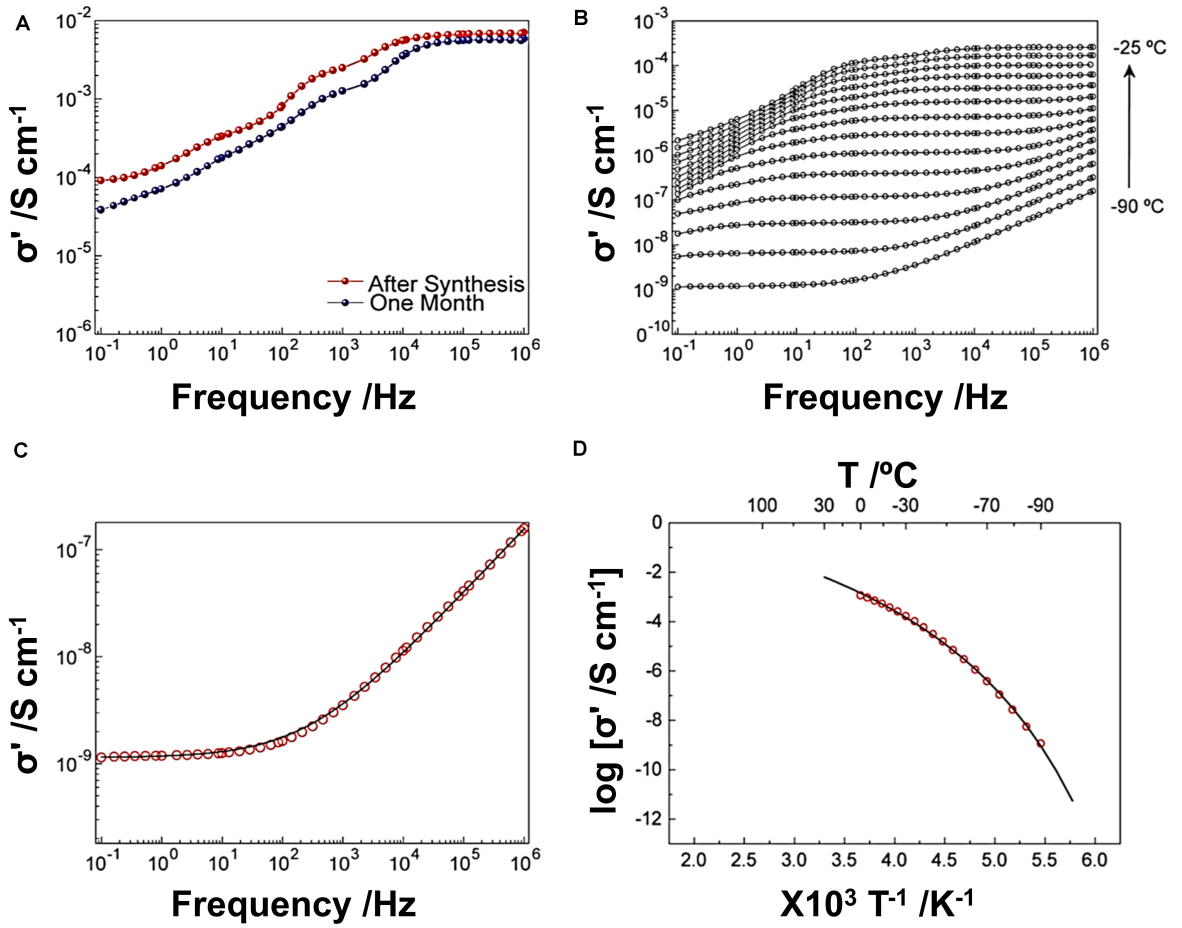

FIGURE 4 | (A) Conductivity at room temperature of CSE after synthesis and after one month, **(B)** conductivity of CSE from −90 °C to −25 °C, with a step of 5 °C, **(C)** Jonscher fit for −90 °C, and **(D)** Thermal evolution of conductivity of CSE.

to the conductivity data, which usually describes the temperature dependence of the electrical conductivity (Eq. 3) quite accurately.

$$\sigma^{'}(T) = \sigma_{\infty} e^{\left(-\frac{B}{T-T_0}\right)} \quad (3)$$

σ_8 is the conductivity in the high-temperature limit, B is an empirical parameter characteristic of the material accounting for the deviation of linearity (roughly B is lower with the more curve dependence), and T_0 is the Vogel temperature as defined for the dependence of relaxation times. The thermal evolution has a non-linear behavior, similar to some other solid electrolytes (Tipton et al., 1994; Alarco et al., 2004; Zhang et al., 2009; Choudhary and Sengwa, 2011; Kamaya et al., 2011; Carvalho et al., 2012).

Despite the similarities in the ionic conductivity behavior with temperature, the contribution of both Li^+ and/or protons in the conduction mechanism is worth discussing. It was been reported that during dissolution of cellulose in the DMAc/LiCl solvent system the Li^+/Cl^- ion pairs split and the Cl^- anions form hydrogen bonds with the hydroxyl protons of cellobiose units (Zhang et al., 2014). This will increase the concentration of free ions when in the solution that would be expected to increase the ionic conductivity. This may be the case in solution but not necessarily in the regenerated membranes, since, during interaction of Cl^- with cellobiose units, the Li^+ cations are solvated by DMAc and accompanied by the hydrogen-bonded Cl^- anions to meet the electric balance (Zhang et al., 2014). Thus, in the formed membranes where cellobiose units are supposed to be fixed, the same is expected to happen to the complex formed by Li^+ ions solvated by remaining DMAc. The DMAc itself is hydrated by the remaining water that will exist in the cellulose electrolytic membranes (Panuszko et al., 2008). That having been said, mobility of Li^+ ions in the CSE membranes is supposed to be limited when compared with highly mobile protons available in the hydration shell of Li^+/DMAc complexes, thus having a more relevant contribution to the ionic conductivity in the CSE membranes. Nevertheless, the existence of Li^+ ions is relevant in fixing the hydrated DMAc that provide a path for proton mobility.

Application in Electrochromic Display

As proof of concept, ECDs were assembled as schematized in **Figure 1** to test the applicability of this new solid-state electrolyte.

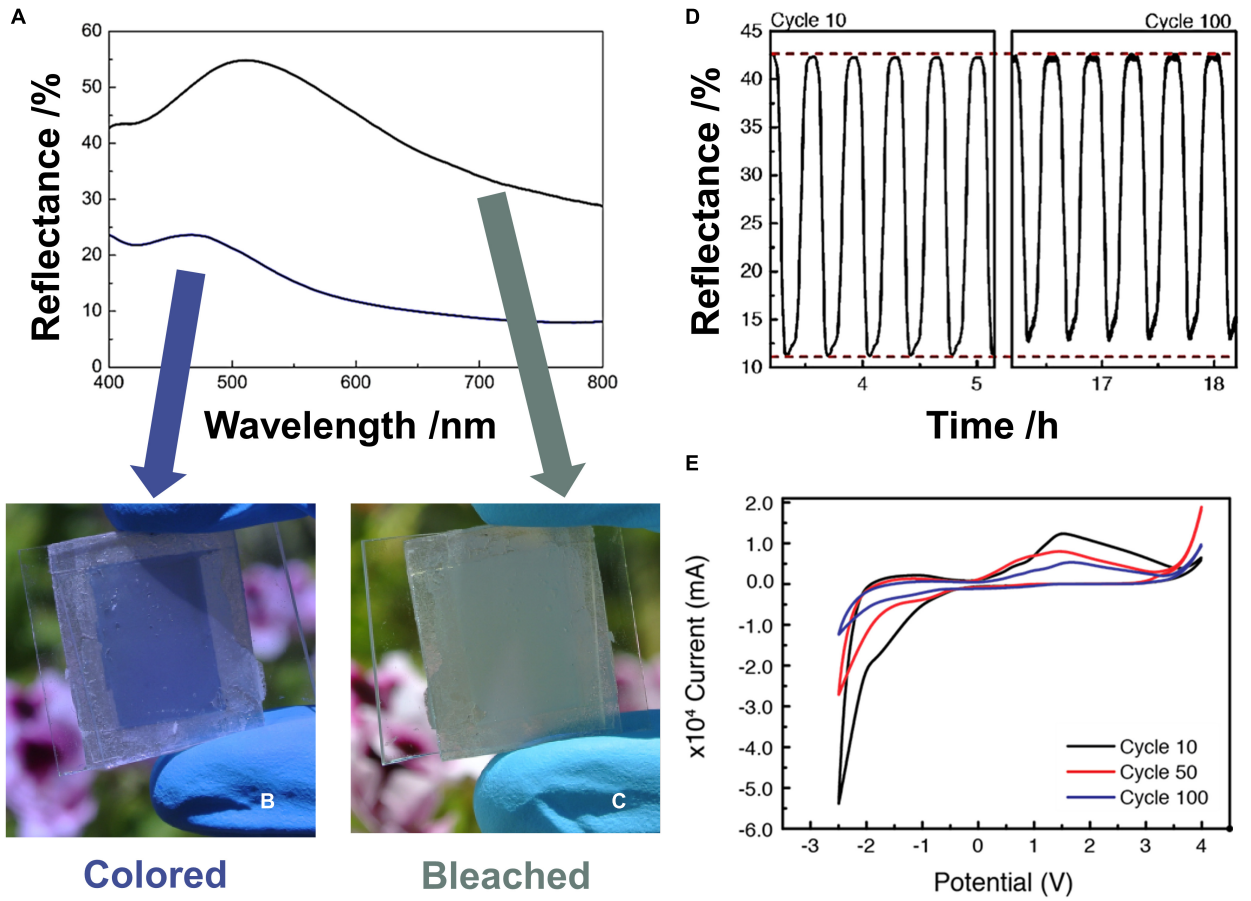

FIGURE 5 | (A) Reflectance and **(B,C)** photographs the ECD in the bleached and colored states. **(D)** Lifetime cycles measurements and **(E)** cyclic voltammograms of the ECD.

The deposition conditions for each layer that constitutes the ECD are described in "Materials and Methods" section. NiO is an anodic electrochromic material that colors under ions deintercalation, changing from a neutral transparency at the bleached state to a dark brown coloration at the colored state (Pereira S. et al., 2014). Because the CSE membrane is partially opaque, in this work, NiO was used only as ion storage layer to keep the charge balance and stability over cycling. On the order hand, WO_3 is a cathodic electrochromic material that colors under ions intercalation changing from transparent on the bleached state to a uniform dark blue when at the colored state (Fernandes et al., 2014), acting here as the electrochromic layer of ECD.

The reflectance and digital photographs of the ECD at the colored and bleached states are presented on **Figures 5a–c**, respectively. Because the CSE is not transparent, the contrast ratio, which is here defined as the reflectance in the bleached state divided by the reflectance in the colored state (Granqvist, 1995), includes only the contribution of the WO_3 layer, even if the NiO also presents electrochromic behavior.

The calculated contrast ratio (at λ = 550 nm) is 36.9%, where the reflectance changes from 52.2% at the bleached state to 15.3% at the colored state. These values are within the expected range of the value as achieved by Silva et al. (2010), with the advantage of using a truly solid, ecofriendly, and less expensive material, with higher conductivity at room temperature. Despite being dependent on the electrochromic material thickness and type, this contrast ratio is also comparable with other ECD incorporating cellulose-based solid electrolytes (Assis et al., 2015; Ngamaroonchote and Chotsuwan, 2016). After 10 coloration/bleaching cycles, the contrast ratio is still 31.5%, slightly decreasing to 30.33% (after 100 cycles), proving that the CSE has excellent stability in the ECD (**Figure 5D**). The decrease in the optical density of the ECD is due to some irreversible ion intercalation. **Figure 5E** shows that, after 100 cycles, the cyclic voltammograms shape for the ECD change. The broad anodic peak remains at the same potential after 50 cycles, but it is moved to a higher potential for the 100th cycle, and their current density values decrease when compared with the values of the 1st cycle.

On the other hand, the cathodic peaks almost completely disappear after the 100th cycle. The changes of cyclic voltammograms observed during cycling of ECD point clearly that redox reactions at WO_3 and NiO are not entirely reversible. As a result, there is a decrease of the charge density values and,

consequently, a decrease of reflectance modulation between color and bleached states. This is mainly due to irreversibility of redox reaction rather than related with the stability of the electrolyte (Assis et al., 2015), which retains its coloration on the area not coated with WO_3 and can be seen on **Figure 4C**.

CONCLUSION

In this work, a new fully cellulose-based solid electrolyte functionalized with lithium ions produced by an easy and reproducible synthesis process was presented. The CSE exhibits a high ionic conductivity of 6.5 $mS.cm^{-1}$ at room temperature, comparable to some liquid electrolytes, and its solid-state nature overcomes the drawbacks related to safety issues of liquid alternatives. The excellent ionic conductivity is attributed to the Li^{+}/DMAc complex formed and retained with the membranes' matrix, which is enhanced by microwave irradiation assisting regenerations the regeneration process. The microwave irradiation also helps in the polymerization of the regenerated membranes that result in better mechanical properties when compared with gel-like sample obtained when no microwave irradiation is used. Additionally, the applicability of this new cellulosic-based electrolyte was demonstrated in an ECD which could open the door for new paper-based displays in the field of disposable paper electronics.

DATA AVAILABILITY STATEMENT

All datasets generated for this study are included in the article/supplementary material.

AUTHOR CONTRIBUTIONS

PD and LP: conceptualization. PD, EF, RM, and LP: methodology. PD, SP, IC, AP, and MD: data curation. PD, SP, IC, and AP: investigation. PD, IC, MD, and LP: writing – original draft preparation. EF, RM, and LP: project administration and funding acquisition. All authors: writing – review and editing.

FUNDING

The authors would like to acknowledge the European Commission under project NewFun (ERC-StG-2014, GA 640598) and BET-EU (H2020-TWINN-2015, GA 692373). This work was also supported by the FEDER funds through the COMPETE 2020 Program and the National Funds through the FCT – Portuguese Foundation for Science and Technology under the Project No. POCI-01-0145-FEDER-007688, Reference UID/CTM/50025, project PapEl, reference PTDC/CTM-NAN/5172/2014 and project CHIHC, reference PTDC/NAN-MAT/32558/2017.

REFERENCES

Ahn, C.-Y., Ahn, J., Kang, S. Y., Kim, O.-H., Lee, D. W., Lee, J. H., et al. (2020). Enhancement of service life of polymer electrolyte fuel cells through application of nanodispersed ionomer. *Sci. Adv.* 6:eaaw0870. doi: 10.1126/sciadv.aaw0870

Alarco, P.-J., Abu-Lebdeh, Y., Abouimrane, A., and Armand, M. (2004). The plastic-crystalline phase of succinonitrile as a universal matrix for solid-state ionic conductors. *Nat. Mater.* 3, 476–481. doi: 10.1038/nmat1158

Amici, J., Romanin, S., Alidoost, M., Versaci, D., Francia, C., Smeacetto, F., et al. (2019). UV-cured methacrylate based polymer composite electrolyte for metallic lithium batteries. *J. Electroanal. Chem.* 837, 103–107. doi: 10.1016/j.jelechem.2019.02.027

Asghar, A., Abdul Samad, Y., Singh Lalia, B., and Hashaikeh, R. (2012). PEG based quasi-solid polymer electrolyte: mechanically supported by networked cellulose. *J. Memb. Sci.* 421–422, 85–90. doi: 10.1016/j.memsci.2012.06.037

Assis, L. M. N., Sabadini, R. C., Santos, L. P., Kanicki, J., Łapkowski, M., and Pawlicka, A. (2015). Electrochromic device with Prussian blue and HPC-based electrolyte. *Electrochim. Acta* 182, 878–883. doi: 10.1016/j.electacta.2015.09.133

Carvalho, T., Augusto, V., Brás, A. R., Lourenço, N. M. T., Afonso, C. A. M., Barreiros, S., et al. (2012). Understanding the Ion Jelly Conductivity Mechanism. *J. Phys. Chem. B.* 116, 2664–2676. doi: 10.1021/jp2108768

Chen, Y., Shi, Y., Liang, Y., Dong, H., Hao, F., Wang, A., et al. (2019). Hyperbranched PEO-based hyperstar solid polymer electrolytes with simultaneous improvement of ion transport and mechanical strength. *ACS Appl. Energy Mater.* 2, 1608–1615. doi: 10.1021/acsaem.8b02188

Chiappone, A., Nair, J. R., Gerbaldi, C., Bongiovanni, R., and Zeno, E. (2013). Nanoscale microfibrillated cellulose reinforced truly-solid polymer electrolytes for flexible, safe and sustainable lithium-based batteries. *Cellulose* 20, 2439–2449. doi: 10.1007/s10570-013-0002-8

Choudhary, S., and Sengwa, R. J. (2011). Dielectric relaxation spectroscopy and ion conduction in poly(ethylene oxide)-blend salts-montmorillonite nanocomposite electrolytes. *Indian J. Pure Appl. Phys.* 49, 204–213. doi: 123456789/11154

Choudhury, S., Stalin, S., Vu, D., Warren, A., Deng, Y., Biswal, P., et al. (2019). Solid-state polymer electrolytes for high-performance lithium metal batteries. *Nat. Commun.* 10:4398. doi: 10.1038/s41467-019-12423-y

Cunha, I., Barras, R., Grey, P., Gaspar, D., Fortunato, E., Martins, R., et al. (2017). Reusable cellulose-based hydrogel sticker film applied as gate dielectric in paper electrolyte-gated transistors. *Adv. Funct. Mater.* 27:1606755. doi: 10.1002/adfm.201606755

Du, Z., Su, Y., Qu, Y., Zhao, L., Jia, X., Mo, Y., et al. (2019). A mechanically robust, biodegradable and high performance cellulose gel membrane as gel polymer electrolyte of lithium-ion battery. *Electrochim. Acta.* 299, 19–26. doi: 10.1016/j.electacta.2018.12.173

Fan, L.-Z., Hu, Y.-S., Bhattacharyya, A. J., and Maier, J. (2007). Succinonitrile as a versatile additive for polymer electrolytes. *Adv. Funct. Mater.* 17, 2800–2807. doi: 10.1002/adfm.200601070

Fan, W., Li, N.-W., Zhang, X., Zhao, S., Cao, R., Yin, Y., et al. (2018). A dual-salt gel polymer electrolyte with 3D cross-linked polymer network for dendrite-free lithium metal batteries. *Adv. Sci.* 5:1800559. doi: 10.1002/advs.201800559

Fernandes, M., Freitas, V. T., Pereira, S., Fortunato, E., Ferreira, R. A. S., Carlos, L. D., et al. (2014). Green Li+- and Er3+-doped poly(ε-caprolactone)/siloxane biohybrid electrolytes for smart electrochromic windows. *Sol. Energy Mater. Sol. Cells.* 123, 203–210. doi: 10.1016/j.solmat.2014.01.011

Garino, N., Zanarini, S., Bodoardo, S., Nair, J. R., Pereira, S., Pereira, L., et al. (2013). Fast switching electrochromic devices containing optimized BEMA/PEGMA gel polymer electrolytes. *Int. J. Electrochem.* 2013, 1–10. doi: 10.1155/2013/138753

Gerbaldi, C., Nair, J. R., Meligrana, G., Bongiovanni, R., Bodoardo, S., and Penazzi, N. (2009). Highly ionic conducting methacrylic-based gel-polymer electrolytes by UV-curing technique. *J. Appl. Electrochem.* 39, 2199–2207. doi: 10.1007/s10800-009-9805-6

Granqvist, C. G. (1995). *Handbook of Inorganic Electrochromic Materials*. Amsterdam: Elsevier. doi: 10.1016/B978-044489930-9/50014-3

Han, J. H., Lee, J. Y., Suh, D. H., Hong, Y. T., and Kim, T.-H. (2017). Electrode-impregnable and cross-linkable Poly(ethylene oxide)–Poly(propylene oxide)–Poly(ethylene oxide) triblock polymer electrolytes with high ionic conductivity

and a large voltage window for flexible solid-state Supercapacitors. *ACS Appl. Mater. Interfaces* 9, 33913–33924. doi: 10.1021/acsami.7b09909

Irimia-Vladu, M. (2014). "Green" electronics: biodegradable and biocompatible materials and devices for sustainable future. *Chem. Soc. Rev.* 43, 588–610. doi: 10.1039/C3CS60235D

Ji, X., Zeng, H., Gong, X., Tsai, F., Jiang, T., Li, R. K. Y., et al. (2017). A Si-doped flexible self-supporting comb-like polyethylene glycol copolymer (Si-PEG) film as a polymer electrolyte for an all solid-state lithium-ion battery. *J. Mater. Chem.* A. 5, 24444–24452. doi: 10.1039/C7TA07741F

Jonscher, A. K. (1990). The "universal" dielectric response. Part I. *IEEE Electr. Insul. Mag.* 6, 16–22. doi: 10.1109/57.50801

Kamaya, N., Homma, K., Yamakawa, Y., Hirayama, M., Kanno, R., Yonemura, M., et al. (2011). A lithium superionic conductor. *Nat. Mater.* 10, 682–686. doi: 10.1038/nmat3066

Kotov, N., Raus, V., and Dybal, J. (2018). Intermolecular interactions in N, N -dimethylacetamide without and with LiCl studied by infrared Spectroscopy and quantum chemical model calculations. *J. Phys. Chem. B.* 122, 8921–8930. doi: 10.1021/acs.jpcb.8b05569

Kremer, F., and Schönhals, A. (2003). *Broadband Dielectric Spectroscopy*. Berlin: Springer International Publishing. doi: 10.1007/978-3-642-56120-7

Lalia, B. S., Samad, Y. A., and Hashaikeh, R. (2014). Ternary polymer electrolyte with enhanced ionic conductivity and thermo-mechanical properties for lithium-ion batteries. *Int. J. Hydrogen Energy.* 39, 2964–2970. doi: 10.1016/j.ijhydene.2013.04.045

Ledwon, P., Andrade, J. R., Lapkowski, M., and Pawlicka, A. (2015). Hydroxypropyl cellulose-based gel electrolyte for electrochromic devices. *Electrochim. Acta.* 159, 227–233. doi: 10.1016/j.electacta.2015.01.168

Li, P., Zhang, Y., Fa, W., Zhang, Y., and Huang, B. (2011). Synthesis of a grafted cellulose gel electrolyte in an ionic liquid ([Bmim]I) for dye-sensitized solar cells. *Carbohydr. Polym.* 86, 1216–1220. doi: 10.1016/j.carbpol.2011.06.017

Liu, R., Wu, Z., He, P., Fan, H., Huang, Z., Zhang, L., et al. (2019). A self-standing, UV-cured semi-interpenetrating polymer network reinforced composite gel electrolytes for dendrite-suppressing lithium ion batteries. *J. Mater.* 5, 185–194. doi: 10.1016/j.jmat.2018.12.006

Łojewska, J., Miśkowiec, P., Łojewski, T., and Proniewicz, L. M. (2005). Cellulose oxidative and hydrolytic degradation: in situ FTIR approach. *Polym. Degrad. Stab.* 88, 512–520. doi: 10.1016/j.polymdegradstab.2004.12.012

Mahadeva, S. K., Yeol Yang, S., and Kim, J. (2013). Effects of solvent systems on its structure, properties and electromechanical behavior of cellulose electro-active paper. *Curr. Org. Chem.* 17, 83–88. doi: 10.2174/138527213805289114

Ngamaroonchote, A., and Chotsuwan, C. (2016). Performance and reliability of cellulose acetate-based gel electrolyte for electrochromic devices. *J. Appl. Electrochem.* 46, 575–582. doi: 10.1007/s10800-016-0918-4

Ni, J., Na, H., She, Z., Wang, J., Xue, W., and Zhu, J. (2014). Responsive behavior of regenerated cellulose in hydrolysis under microwave radiation. *Bioresour. Technol.* 167, 69–73. doi: 10.1016/j.biortech.2014.05.066

Nketia-Yawson, B., Tabi, G. D., and Noh, Y.-Y. (2019). Polymer electrolyte blend gate dielectrics for high-performance ultrathin organic transistors: toward favorable polymer blend miscibility and reliability. *ACS Appl. Mater. Interfaces.* 11, 17610–17616. doi: 10.1021/acsami.9b03999

Panuszko, A., Gojło, E., Zielkiewicz, J., Śmiechowski, M., Krakowiak, J., and Stangret, J. (2008). Hydration of simple amides. FTIR Spectra of HDO and theoretical studies. *J. Phys. Chem. B.* 112, 2483–2493. doi: 10.1021/jp7099509

Pereira, L., Gaspar, D., Guerin, D., Delattre, A., Fortunato, E., and Martins, R. (2014). The influence of fibril composition and dimension on the performance of paper gated oxide transistors. *Nanotechnology* 25:094007. doi: 10.1088/0957-4484/25/9/094007

Pereira, S., Gonçalves, A., Correia, N., Pinto, J., Pereira, L., Martins, R., et al. (2014). Electrochromic behavior of NiO thin films deposited by e-beam evaporation at room temperature. *Sol. Energy Mater. Sol. Cells.* 120, 109–115. doi: 10.1016/j.solmat.2013.08.024

Ramos, A. M., Pereira, S., Cidade, M. T., Pereira, G., Branquinho, R., Pereira, L., et al. (2013). Preparation and characterization of cellulose nanocomposite hydrogels as functional electrolytes. *Solid State Ionics* 242, 26–32. doi: 10.1016/j.ssi.2013.03.028

Samad, Y. A., Asghar, A., and Hashaikeh, R. (2013). Electrospun cellulose/PEO fiber mats as a solid polymer electrolytes for Li ion batteries. *Renew. Energy* 56, 90–95. doi: 10.1016/j.renene.2012.09.015

Segal, L., Creely, J. J., Martin, A. E., and Conrad, C. M. (1959). An empirical method for estimating the degree of crystallinity of native cellulose using the X-ray diffractometer. *Text. Res. J.* 29, 786–794. doi: 10.1177/004051755902901003

Silva, M. M., Barbosa, P. C., Rodrigues, L. C., Gonçalves, A., Costa, C., and Fortunato, E. (2010). Gelatin in electrochromic devices. *Opt. Mater.* 32, 719–722. doi: 10.1016/j.optmat.2009.08.013

Sun, B., Duan, L., Peng, G., Li, X., and Xu, A. (2015). Efficient production of glucose by microwave-assisted acid hydrolysis of cellulose hydrogel. *Bioresour. Technol.* 192, 253–256. doi: 10.1016/j.biortech.2015.05.045

Tipton, A. L., Lonergan, M. C., Ratner, M. A., Shriver, D. F., Wong, T. T. Y., and Han, K. (1994). Conductivity and Dielectric Constant of PPO and PPO-Based Solid Electrolytes from Dc to 6 GHz. *J. Phys. Chem.* 98, 4148–4154. doi: 10.1021/j100066a039

Vidinha, P., Lourenço, N. M. T., Pinheiro, C., Brás, A. R., Carvalho, T., Santos-Silva, T., et al. (2008). Ion jelly: a tailor-made conducting material for smart electrochemical devices. *Chem. Commun.* 30, 5842–5844. doi: 10.1039/b811647d

Wang, Y., Li, B., Ji, J., Eyler, A., and Zhong, W. H. (2013). A gum-like electrolyte: safety of a solid, performance of a liquid. *Adv. Energy Mater.* 3, 1557–1562. doi: 10.1002/aenm.201300495

Xue, Z., He, D., and Xie, X. (2015). Poly(ethylene oxide)-based electrolytes for lithium-ion batteries. *J. Mater. Chem.* A. 3, 19218–19253. doi: 10.1039/C5TA03471J

Yildirim, A., Szymoniak, P., Sentker, K., Butschies, M., Bühlmeyer, A., Huber, P., et al. (2018). Dynamics and ionic conductivity of ionic liquid crystals forming a hexagonal columnar mesophase. *Phys. Chem. Chem. Phys.* 20, 5626–5635. doi: 10.1039/C7CP08186C

Zhang, C., Gamble, S., Ainsworth, D., Slawin, A. M. Z., Andreev, Y. G., and Bruce, P. G. (2009). Alkali metal crystalline polymer electrolytes. *Nat. Mater.* 8, 580–584. doi: 10.1038/nmat2474

Zhang, C., Liu, R., Xiang, J., Kang, H., Liu, Z., and Huang, Y. (2014). Dissolution mechanism of cellulose in N,N -Dimethylacetamide/Lithium chloride: revisiting through molecular interactions. *J. Phys. Chem. B.* 118, 9507–9514. doi: 10.1021/jp506013c

Zhang, J., Liu, Z., Kong, Q., Zhang, C., Pang, S., Yue, L., et al. (2013). Renewable and superior thermal-resistant cellulose-based composite nonwoven as lithium-ion battery separator. *ACS Appl. Mater. Interfaces.* 5, 128–134. doi: 10.1021/am302290n

Zhang, Q., Liu, K., Ding, F., Li, W., Liu, X., and Zhang, J. (2017). Safety-reinforced succinonitrile-based electrolyte with interfacial stability for high-performance lithium batteries. *ACS Appl. Mater. Interfaces* 9, 29820–29828. doi: 10.1021/acsami.7b09119

Zhang, X., Wang, X., Liu, S., Tao, Z., and Chen, J. (2018). A novel PMA/PEG-based composite polymer electrolyte for all-solid-state sodium ion batteries. *Nano Res.* 11, 6244–6251. doi: 10.1007/s12274-018-2144-3

Zhao, L., Fu, J., Du, Z., Jia, X., Qu, Y., Yu, F., et al. (2020). High-strength and flexible cellulose/PEG based gel polymer electrolyte with high performance for lithium ion batteries. *J. Memb. Sci.* 593:117428. doi: 10.1016/j.memsci.2019.117428

Zhu, M., Yu, L., He, S., Hong, H., Liu, J., Gan, L., et al. (2019). highly efficient and stable cellulose-based ion gel polymer electrolyte for solid-state Supercapacitors. *ACS Appl. Energy Mater.* 2, 5992–6001. doi: 10.1021/acsaem.9b01109

Conflict of Interest: The authors declare that the research was conducted in the absence of any commercial or financial relationships that could be construed as a potential conflict of interest.